divided the zeolites into two, somewhat artificial, classes: group I, systems of [Si/Al] ratios from 1 to 3, typified by structures dominated by interlaced tetrahedral silica aluminate cages, e.g., A, X, Y, and L zeolites; and group II, systems of large [Si/Al] ratio from 5 to > 100, typified by structures dominated by interlaced chains, e.g., mordenite, ZSM-5, and silicalite.

The valence band spectra exhibited by these zeolite systems are *not* just additive renditions of that for silica and for alumina, but rather the zeolite spectra reveal complex shiftings and alterations.

In addition, the valence band results for the group II systems appear to be quite similar in appearance to silica, suggesting a silica-dominated system with increasing aluminate perturbation as the [Si/Al] ratio decreases, i.e., silicalite < ZSM-5 < mordenite. There is a rather abrupt and not entirely understood change in the detected valence band structure after mordenite, as the [Si/Al] ratio decreases, perhaps suggesting a recognition by the ESCA of a difference between the aforementioned chain-like structures with large [Si/Al] (II), compared to the cage-like structures with [Si/Al] ratios between 3 and 1 (I).

The valence band results for all of the group I zeolites are shown to produce three principal subband regions, with a number of peaks detected in each. Based upon a variety of results, calculations, and other supportive information, suppositional identifications are made of each of these peaks. In this manner, the bonding and nonbonding character of these zeolites are broken down, analyzed, and compared. It is suggested, for example, that the relative ionicity (polarity) of the zeolites increases inversely with the [Si/Al] ratio, with the silica covalency of the NaA system so depleted that it seems more appropriate to describe it as a partially ionic sodium aluminate, perturbed by silica. In all cases, the subbands shift and contract dramatically from those for the "precursor" systems (silica and sodium aluminate), suggesting that the substitution of the latter into the tetrahedral silica lattice substantially perturbs the electronic structure of the silica, but does so through the interjection of *group* ($NaAlO_2$), rather than elemental (ESCA) *shifts*.

Suppositional arguments are presented to explain the spectral distinction between group I and II systems based on both structural and compositional factors. Lowenstein's rule is also employed, but the extent of its application is hard to determine.

Consideration is also given for the description of these materials in terms of the Green's function based amalgamation/persistence models of Onodera and Toyozawa.[37] It is argued that the zeolites, in question, should fall into the amalgamation category, but those in group I fail to do so properly without the inclusion of additional terms in the Green's functions to describe the covalent and/or ionic bonding that seems to prohibit the zeolites from being simple solid solutions of SiO_2 and $NaAlO_2$. This model does seem to provide an explanation of the valence bands of the group II zeolites based on the perturbation of the silica lattice by varying amounts of aluminate.

Useful information has also been extracted from studies of the behavior of zeolite valence bands during change of cations, selective sputter etching, catalytic abuses, thermal treatment, etc. The details of these studies are presented in other publications.[9,11,32,35]

Characterization and Novel Low-Temperature Reactions of $FeCH_2$ and N_2FeCH_2

Sou-Chan Chang, Robert H. Hauge, Zakya H. Kafafi, John L. Margrave,* and W. E. Billups*

Contribution from the Department of Chemistry, Rice University, Houston, Texas 77251.
Received March 21, 1988

Abstract: The reactions of iron atoms with diazomethane have been investigated in argon matrices by FTIR matrix isolation spectroscopy. These studies show that iron atoms insert spontaneously into diazomethane to yield $FeCH_2$ and N_2FeCH_2. Photolysis of the matrix at $\lambda \geq 500$ nm leads to the reductive elimination of iron from N_2FeCH_2. UV photolysis of the matrix results in the facile conversion of $FeCH_2$ to HFeCH, whereas photolysis of the carbyne through a cutoff filter with $\lambda \geq 400$ nm leads to the reverse process. $FeCH_2$ and N_2FeCH_2 react with dihydrogen to yield CH_3FeH and N_2CH_3FeH, respectively, with N_2FeCH_2 reacting more rapidly than $FeCH_2$. $FeCH_2$ was found to react with water to yield CH_3FeOH.

Although carbene complexes are recognized as important intermediates in a large number of catalytic reactions, only a limited number of instances have been reported in which authentic carbene intermediates have been used to initiate the catalytic cycle. In most instances this can be attributed to the short lifetime and low concentration of the intermediate. Accordingly, these systems are usually modeled using fairly stable complexes.[1] FTIR matrix isolation spectroscopy is often used to characterize unstable species present in low concentration. In this paper we describe the synthesis and characterization of $FeCH_2$ and N_2FeCH_2, their reactions with dihydrogen and water, and the photolytic rearrangement of $FeCH_2$ to HFeCH.

Experimental Section

A complete description of the multisurface matrix isolation apparatus has been reported.[2] The preparation of CH_2N_2, CD_2N_2, $CHDN_2$, and $^{13}CH_2N_2$ has also been discussed.[3] Iron atoms (AESAR, 99.98%) were vaporized from an alumina crucible enclosed in a resistively heated tantalum furnace over the range 1300–1500 °C. The temperature of the furnace was measured with a microoptical pyrometer (Pyrometer Instrument Co.).

In a typical experiment, iron atoms and diazomethane were cocondensed with argon (Matheson, 99.9998%) or nitrogen (Matheson, 99.9995%) onto a rhodium-plated copper surface at 11–14 K over a period of 30 min. Prior to deposition, the molar ratio of iron, diazomethane, and matrix gas was measured with a quartz crystal microbalance mounted on the cold block. During deposition the rate of effusion of iron was continuously monitored with a water-cooled quartz crystal microbalance situated at the back of the furnace. In this study the molar ratio of iron to matrix gas was varied from 0 to 23 parts per thousand and the ratio of diazomethane to matrix gas was varied from 0 to 15 parts

(1) See: *Transition Metal Carbene Complexes*; Verlag Chemie: Weinheim, 1983.

(2) Hauge, R. H.; Fredin, L.; Kafafi, Z. H.; Margrave, J. L. *Appl. Spectrosc.* **1986**, *40*, 588.

(3) Chang, S.-C.; Kafafi, Z. H.; Hauge, R. H.; Billups, W. E.; Margrave, J. L. *J. Am. Chem. Soc.* **1987**, *109*, 4508.

0002-7863/88/1510-7975$01.50/0

Table I. Measured and Calculated Infrared Frequencies (cm^{-1}) of $FeCH_2$, $Fe^{13}CH_2$, FeCHD, and $FeCD_2$ in Solid Argon

vibrational mode	$FeCH_2$		$Fe^{13}CH_2$		FeCHD		$FeCD_2$	
	obsd	calcd	obsd	calcd	obsd	calcd	obsd	calcd
CH_2, CD_2 s stretch	2941.6	2941.6	2936.1	2936.1		2168.3	2134.3	2134.3
CHD CD stretch								
CH_2, CD_2[a]		1319.2		1312.2		1175.2		1004.0
CHD bend								
Fe=C, Fe=^{13}C stretch	623.9	624.0	607.7	608.1	608.2	608.9	575.2	573.6
CH_2, CD_2 a stretch	3011.5	3010.7	3002.0	3002.8	2975.9	2975.9	2201.0	2201.2
CDH CH stretch								
CH_2, CD_2	452.0	452.4	449.1	449.3	382.0	382.2	347.6	346.8
CHD rock								
CH_2, CD_2	700.3	701.1	694.2	695.0	629.4	629.7	552.7	549.1
CHD wag	697.4		691.4		628.0		550.9	

[a] The CH_2 and CD_2 bending bands were not observed in Ar matrices. The calculated values reported here were derived from the same mode exhibited by $(N_2)_xFeCH_2$ in nitrogen matrices.

per thousand. After deposition, the infrared spectrum of the matrix isolated species was measured with an IBM IR-98 Fourier-transform infrared spectrometer. The frequencies were measured over the range 4000–300 cm^{-1} to an accuracy of ±0.05 cm^{-1}.

Hydrogenation of the matrix isolated species was carried out by introducing dihydrogen (Air Products, 99.9995%) or dideuterium (Air Products, 99.99%) (H_2 or D_2/Ar ≈ 15–50 mmHg/1000 mmHg) into the system during the 30-min deposition. This experiment was usually carried out immediately after a regular deposition process as described above. Hydrolysis reactions were carried out similarly by cocondensing H_2O or D_2O (Sigma, 99.8 atom % D) with iron atoms, diazomethane, and argon. The molar ratio of H_2O or D_2O/Ar was about 5/1000.

Matrices were usually irradiated subsequent to deposition by exposure to a focused 100-W medium-pressure short-arc Hg lamp. The typical exposure time was 10 min. A water filter with various Corning long-pass cutoff filters and a band filter, 280–360 nm, were used for the wavelength-dependent photolysis experiments.

Results and Discussion

Two major products, $FeCH_2$ and N_2FeCH_2, were formed spontaneously when iron atoms and diazomethane were cocondensed with argon.[4] The infrared spectra of these two products

$$Fe + CH_2N_2 \xrightarrow[12\ K]{Ar} \begin{cases} Fe{=}CH_2 + N_2 \\ N_2Fe{=}CH_2 \end{cases}$$

(labeled a and b, respectively) obtained from an iron concentration study are presented in Figure 1. In this study the CH_2N_2/Ar molar ratio was kept constant at 0.98/100 as the Fe/Ar molar ratio was increased from 0.0 to 2.3%.

A number of other features are also present in the spectra of Figure 1. For example, bands labeled c can be assigned to N≡N stretching absorptions. Those found in the 2000–2300-cm^{-1} region have been assigned previously to $Fe_2(N_2)_x$ species.[5] The band labeled c at 1827.0 cm^{-1} was found to arise from a diiron complex which can be produced from either iron/diazomethane/argon or iron/dinitrogen/argon matrices. The stoichiometry of iron for each species was determined by a log–log plot of the intensities of absorption of selected bands versus iron concentration[6] as depicted in Figure 2.

Table II. Molecular Geometry, Symmetry Coordinates, and Force Constants Used for $FeCH_2$, $Fe^{13}CH_2$, FeCHD, and $FeCD_2$ in the Normal Coordinate Analyses

	$r_1 = r_2 = r$(C–H) = 1.07 Å	F_{11} = 4.897 mdyn/Å
	$r_3 = r$(Fe–C) = 1.9 Å	F_{12} = 0.410 mdyn/Å
	$\phi_1 = \phi_2 = \angle$(FeCH) = 123.5°	F_{13} = –0.070 mdyn/rad
	$\phi_3 = \angle(CH_2)$ = 113°	F_{22} = 2.651 mdyn/Å
	$\theta_1 = \angle(FeCH_2)$ = 180.0°	F_{23} = –0.006 mdyn/rad
		F_{33} = 0.348 mdyn Å/rad^2
A′	$S_1 = 2^1/_2(\Delta r_1 + \Delta r_2)$	F_{44} = 4.902 mdyn/Å
	$S_2 = \Delta r_3$	F_{45} = 0.788 mdyn/rad
	$S_3 = 6^1/_2(2\Delta\phi_1 - \Delta\phi_2 - \Delta\phi_3)$	F_{55} = 0.241 mdyn Å/rad^2
	$S_4 = 2^1/_2(\Delta r_1 - \Delta r_2)$	F_{66} = 0.157 mdyn Å/rad^2
	$S_5 = 2^1/_2(\Delta\phi_2 - \Delta\phi_3)$	
A″	$S_6 = \Delta\theta_1 \sin \phi_1$	

Table III. Measured Infrared Frequencies (cm^{-1}) of N_2FeCH_2, $N_2Fe^{13}CH_2$, N_2FeCHD, and N_2FeCD_2 in Solid Argon

vibrational mode	N_2FeCH_2	$N_2Fe^{13}CH_2$	N_2FeCHD	N_2FeCD_2
CH_2, CD_2 s stretch CD stretch of CHD	2925.2	2919.2		
CH_2, CD_2 a stretch CH stretch of CHD	2980.0	2970.3	2952.2	
CH_2, CD_2, CHD rock	543.6	540.7		
CH_2, CD_2, CHD wag	733.8	726.6	669.0	590.8
N≡N stretch	1812.0	1812.0	1812.0	1812.3

The peaks labeled d have been shown to arise from reactions with residual dihydrogen. Studies with dihydrogen as a ternary reagent are discussed below.

The infrared spectra of $FeCH_2$, N_2FeCH_2, and isotopically labeled species are presented in Figure 3. Normal coordinate analyses have been carried out on each isotopically labeled species of $FeCH_2$. The observed and calculated frequencies for each of these compounds are presented in Table I. The good agreement between calculated and observed values confirm the vibrational mode assignments. The molecular geometries used in these calculations and the calculated force constants are presented in Table II. Similar assignments for N_2FeCH_2 are presented in Table III. The low N≡N stretching frequency of N_2FeCH_2 at 1812.3 cm^{-1} may indicate that the dinitrogen is bound "side-on", as the more common "end-on" form usually absorbs above 2000 cm^{-1}.[7,8] Further experiments using $^{15}N_2CH_2$ and $^{15}N^{14}NCH_2$

(4) The characterization of $FeCH_2$ has been described in a preliminary communication. See: Chang, S.-C.; Kafafi, Z. H.; Hauge, R. H.; Billups, W. E.; Margrave, J. L. *J. Am. Chem. Soc.* **1985**, *107*, 1447. For other related work see: Chang, S.-C.; Hauge, R. H.; Kafafi, Z. H.; Margrave, J. L.; Billups, W. E. *Chem. Commun.* **1987**, 1682, and ref 3.

(5) Barrett, P. H.; Montano, P. A. *J. Chem. Soc., Faraday Trans. 2* **1977**, *73*, 378.

(6) Moskovits, M., Ed. *Metal Clusters*, Wiley Interscience: New York, 1986.

(7) Ozin, G. A.; Vander Voet, A. *Can. J. Chem.* **1973**, *51*, 637.

(8) Foosnaes, T.; Pellin, M. J.; Gruen, D. M. *J. Chem. Phys.* **1983**, *78*, Part 1, 2889.

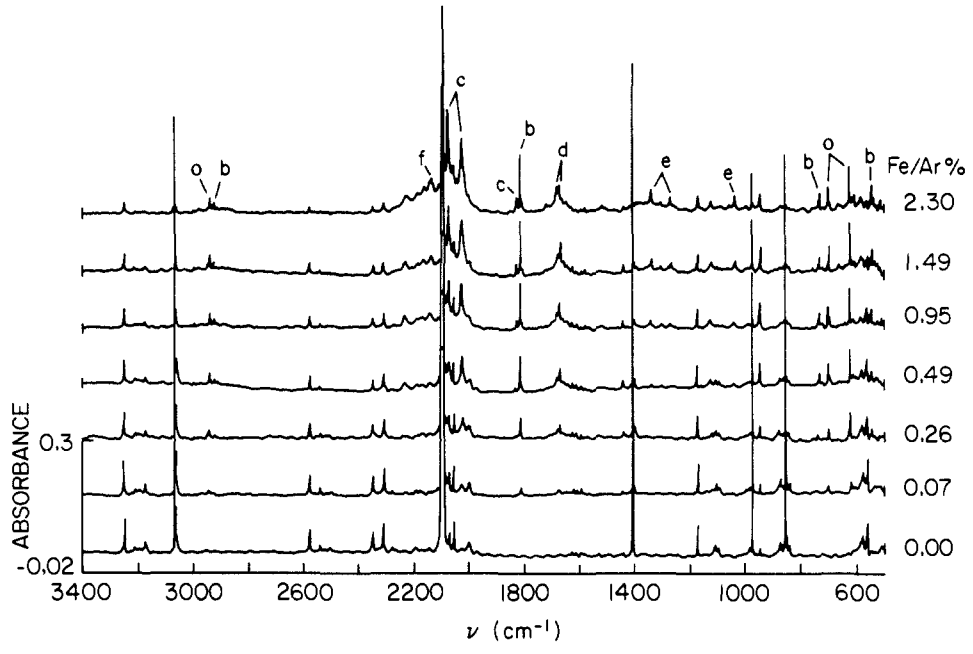

Figure 1. An iron concentration study. Molar ratio of $CH_2N_2/Ar \simeq 0.98/100$: (a) $FeCH_2$, (b) N_2FeCH_2, (c) $Fe_2(N_2)x$ complexes, (d) CH_3FeH and $(N_2)CH_3FeH$, (e) Fe_2/CH_2N_2 reaction products, and (f) CO.

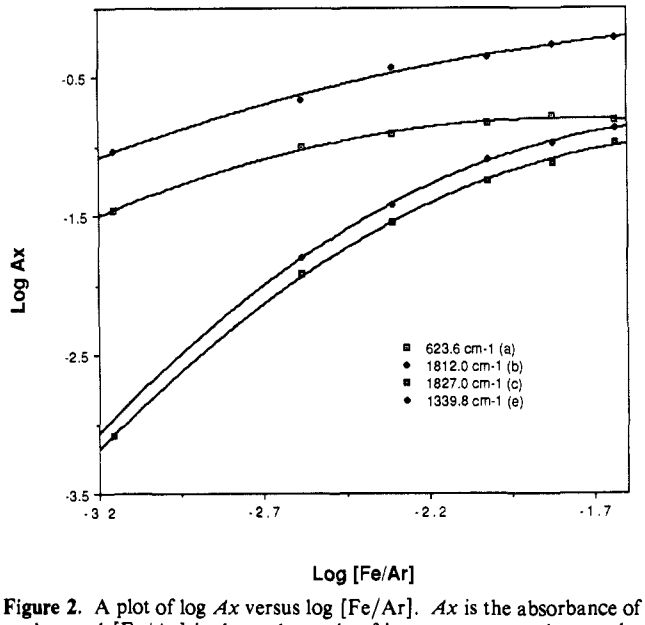

Figure 2. A plot of log Ax versus log [Fe/Ar]. Ax is the absorbance of peak x and [Fe/Ar] is the molar ratio of iron to argon: a, b, c, and e refer to the absorptions of $FeCH_2$, N_2FeCH_2, $Fe_2(N_2)_x$, and Fe_2/CH_2N_2 reaction products, respectively, as shown in Figure 1. At low iron concentration (log [Fe/Ar] = −2.9) the slopes of lines a and b are ≈0.8, whereas the slopes of lines c and line e are ≈2.0.

would be necessary to differentiate between the two forms.

Photolysis of an iron/diazomethane/argon matrix with $\lambda \geq 500$ nm leads to significant bleaching of the bands assigned to N_2-$FeCH_2$; however, no new absorptions associated with a Fe/CH_2N_2 reaction product could be identified. This observation suggests that a reductive elimination reaction may occur with the low-energy photolysis.

$$N_2FeCH_2 \xrightarrow{\lambda \geq 500\ nm} Fe + CH_2N_2$$

Photolysis under the same conditions or with $\lambda \geq 400$ nm irradiation showed little effect on the absorptions arising from $FeCH_2$; however, UV photolysis ($360 \geq \lambda \geq 280$ nm) leads to the rapid conversion of $FeCH_2$ to a new species with absorptions at 1681.6, 674.2, and 632.1 cm^{-1}. These new absorptions are assigned to HFe≡CH. Thus the band at 1681.6 cm^{-1} can be assigned readily to a Fe—H stretching mode. The remaining two bands

Table IV. Measured and Calculated Frequencies (cm^{-1}) of HFeCH, $HFe^{13}CH$, and DFeCD in Solid Argon

	HFeCH		$HFe^{13}CH$		DFeCD	
vibrational mode	obsd	calcd	obsd	calcd	obsd	calcd
Fe≡C, Fe≡^{13}C stretch	674.2	675.2	655.0	655.4	648.3	646.8
FeC–H, FeC–D bend	632.1	635.4	627.6	630.9	503.7	489.6
Fe–H, Fe–D stretch	1681.6	1681.8	1681.6	1681.5	1209.2	1209.0

Table V. Molecular Geometry and Force Constants Used for HFeCH, $HFe^{13}CH$, and DFeCD in the Normal Coordinate Analyses

$r_1 = r$(H–Fe) = 1.6 Å	F_{11} = 1.825 mdyn/Å
$r_2 = r$(Fe–C) = 1.7 Å	F_{12} = −0.608 mdyn/Å
$r_3 = r$(C–H) = 1.07 Å	F_{22} = 2.805 mdyn/Å
$\theta_1 = \angle$(HFeCH) = 0.0°	F_{23} = 0.010 mdyn/Å
	F_{33} = 6.009 mdyn/Å
	F_{44} = 0.214 mdyn Å/rad^2

at 674.2 and 632.1 cm^{-1} are assigned to a Fe≡C stretching mode and a C—H bending mode, respectively. The C—H stretching band of this species was not observed. Photolysis of the carbyne through a cutoff filter with $\lambda \geq 400$ nm leads to the reverse process.

$$FeCH_2 \underset{\lambda \geq 400\ nm}{\overset{UV}{\rightleftharpoons}} HFeCH$$

The infrared spectra of HFeCH, $HFe^{13}CH$, and DFeCD are presented in Figure 4. Good agreement is found between the observed and calculated frequencies for each species (Table IV). The molecular geometries used in the force field calculations are listed in Table V.

This reversible migration of hydrogen between iron and carbon is an interesting process. For example, accurate structures for five-coordinate, 14-electron complexes reveal startling bond angles for these species.[9]

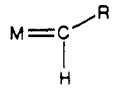

(9) Goddard, R. J.; Hoffmann, R.; Jemmis, E. D. *J. Am. Chem. Soc.* **1980**, *102*, 7667–7676.

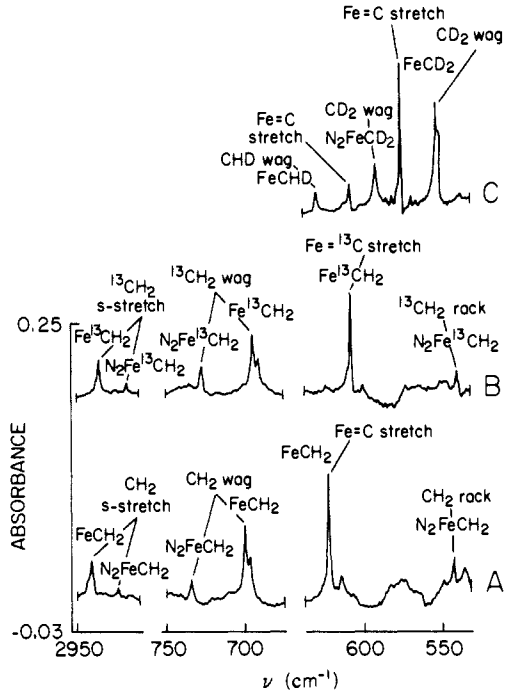

Figure 3. FTIR spectra of selected regions of (A) $FeCH_2$ and N_2FeCH_2; (B) $Fe^{13}CH_2$ and $N_2Fe^{13}CH_2$; (C) FeCHD, $FeCD_2$, and N_2FeCD_2 in argon matrices.

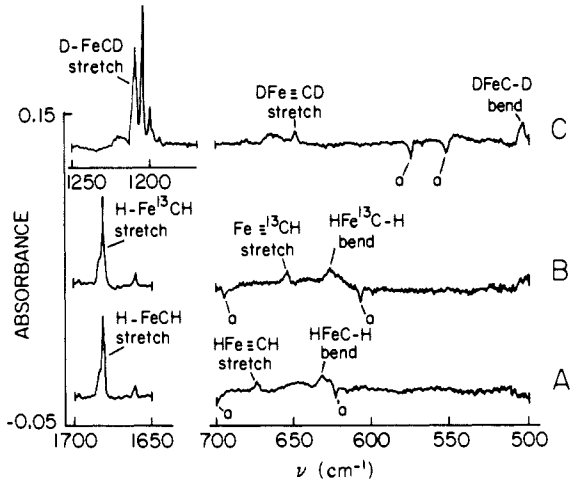

Figure 4. FTIR difference spectra (before and after UV photolysis) in argon matrices of selected regions of (A) HFeCH; (B) $HFe^{13}CH$; (C) DFeCD. a = $FeCH_2$ in A, $Fe^{13}CH_2$ in B, and $FeCD_2$ in C.

One might expect that the apparent M---H interaction responsible for this geometry would facilitate hydrogen transfer to the metal; however, theoretical calculations indicate that the process is forbidden. This symmetry imposed barrier is apparently lifted in the photoinduced rearrangement observed here.

A second salient discovery resulted from the observation that residual hydrogen reacted with $FeCH_2$ to yield CH_3FeH. The observed frequencies of CH_3FeH were found at 1683.6, 1156.1, 541.9, and 537.6 cm^{-1}. These absorptions can be assigned readily to CH_3FeH, since the same species can be prepared by photolysis of a $Fe/CH_4/Ar$ matrix.[10,11] In addition, absorptions at 1672.0, 1153.5, 550.3, 536.1, and 521.9 cm^{-1} were also observed in the $Fe/CH_2N_2/Ar$ matrix. The similarity of these absorptions to those of CH_3FeH suggested that N_2FeCH_2 was also reduced by residual hydrogen. Unfortunately, the absorption of the coordinated nitrogen was obscured by $Fe_2(N_2)_x$ bands. The stronger absorptions of N_2CH_3FeH compared to those of CH_3FeH also, surprisingly, indicate that N_2FeCH_2 is more reactive than $FeCH_2$ toward hydrogenation, an observation not easily rationalized.

These observations were confirmed by carrying out experiments in which excess dihydrogen was cocondensed with the matrix. As shown in Figure 5, this experiment results in a significant increase in the absorptions assigned to N_2CH_3FeH with a concomitant decrease in the N_2FeCH_2 bands without much change in the CH_3FeH absorptions. This observation further supports the finding that N_2FeCH_2 exhibits a greater reactivity toward dihydrogen than $FeCH_2$. The photoinduced reductive elimination/oxidative addition reactions of CH_3FeH[11] and N_2CH_3FeH

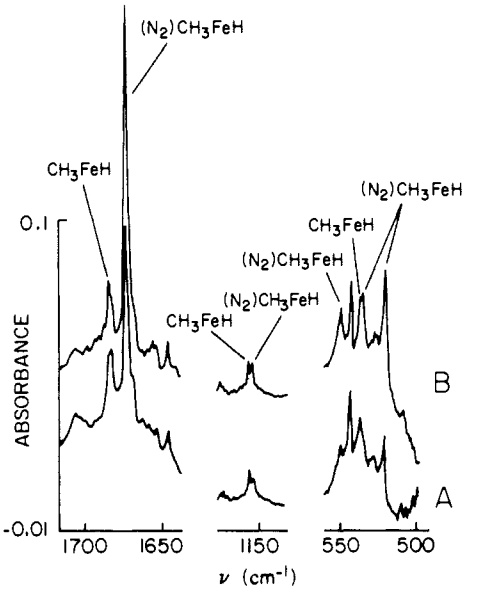

Figure 5. FTIR spectra of selected regions of CH_3FeH and $(N_2)CH_3FeH$ in a matrix hydrogenation reaction: (A) without H_2, $Fe/CH_2N_2/Ar$ = 0.9/1.1/100; (B) with added H_2 during deposition, $Fe/CH_2N_2/H_2/Ar$ = 0.9/1.1/10/100. The products observed in A were due to the reaction with residual hydrogen in the system.

Table VI. Measured Infrared Frequencies (cm^{-1}) of CH_3FeH and Its Isotopically Labeled Species in Solid Argon

		band absorptions			
molecules	reactions	ν(MH) ν(MD)	δ(CH_3) δ(CD_3) δ(CH_2D) δ(CD_2H)	ρ_r(CH_3) ρ_r(CD_3) ρ_r(CH_2D) ρ_r(CD_2H)	ν(MC) ν($M^{13}C$)
CH_3FeH	Fe/CH_4	1683.6 1675.0	1156.1	544.0 541.0	523.5
CH_3FeH	$FeCH_2/H_2$	1683.6	1156.1	541.9 537.6	
$(N_2)CH_3$-FeH	N_2FeCH_2/H_2	1672.0	1153.5	550.3 536.1	521.9
$^{13}CH_3FeH$	$Fe/^{13}CH_4$	1683.6	1147.0	540.2 538.3	510.0
$^{13}CH_3FeH$	$Fe^{13}CH_2/H_2$	1683.6	1147.0		
$(N_2)^{13}CH_3$ FeH	N_2FeCH_2/H_2	1671.7	1145.0	548.2 543.7	510.1
CH_2DFeD	$FeCH_2/D_2$	1211.6	1079.0		
$(N_2)CH_2C$-FeD	N_2FeCH_2/D_2	1203.4	1075.9	539.2 532.0 526.0	
CD_2HFeH	$FeCD_2/H_2$	1683.3			
$(N_2)CD_2H$-FeH	N_2FeCD_2/H_2	1671.7			
CD_3FeD	$FeCD_2/D_2$	1210.8			
$(N_2)CD_3$-FeD	N_2FeCD_2/D_2	1202.8			

(10) Billups, W. E.; Konarski, M. M.; Hauge, R. H.; Hargrave, J. L. *J. Am. Chem. Soc.* **1980**, *102*, 7393.
(11) Ozin, G. A.; McCaffrey, J. C. *J. Am. Chem. Soc.* **1982**, *104*, 7351.

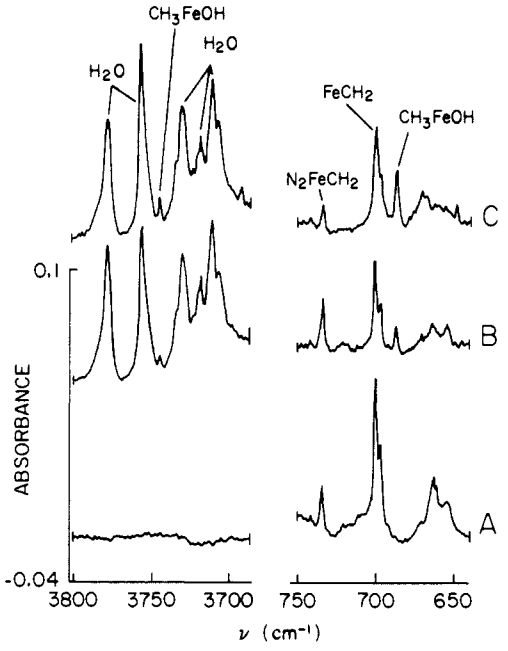

Figure 6. FTIR spectra of selected regions of CH_3FeOH in a matrix hydrolysis reaction: (A) without H_2O, $Fe/CH_2N_2/Ar$ = 0.8/1.1/100; (B) with added H_2O during deposition, $Fe/CH_2N_2/H_2O/Ar$ = 0.8/1.1/0.5/100; (C) after 10-min photolysis of B with $\lambda \geq 500$ nm.

were also observed in this system; however, the effect is very small.

The hydrogenation reaction of $FeCH_2$ and N_2FeCH_2 provides a convenient route to prepare methyl iron hydride from mixed isotopically labeled species which might otherwise be difficult to obtain. For example, CH_2DFeD and $(N_2)CH_2DFeD$ can be obtained from a $Fe/CH_2N_2/D_2/Ar$ reaction, whereas CD_2HFeH and $(N_2)CD_2HFeH$ can be made from a $Fe/CD_2N_2/H_2/Ar$ reaction. The frequencies of various isotopic molecules obtained from $Fe/CH_2N_2/H_2$, $Fe/CH_2N_2/D_2$, $Fe/^{13}CH_2N_2/H_2$, $Fe/CD_2N_2/H_2$, $Fe/CD_2N_2/D_2$, Fe/CH_4, and Fe/CD_4 in argon are listed in Table VI.

Matrix reactions with water have also been carried out. The infrared spectra of a $Fe/CH_2N_2/H_2O/Ar$ reaction are illustrated in Figure 6. The growth of two new peaks at 3744.8 and 687.3 cm^{-1} along with a decrease in the intensities of the absorptions arising from $FeCH_2$ supports the assumption that hydration has occurred. Since these same absorptions have been assigned to an O–H stretching mode and an Fe–O stretching mode of CH_3FeOH in a study of $Fe/CH_3OH/Ar$, the product can be assigned securely as CH_3FeOH.[12] An increase in the product bands after $\lambda \geq 500$ nm photolysis (Figure 6C) indicates that additional reaction occurs probably through photoinduced diffusion of $FeCH_2$ with neighboring H_2O molecules.

The regiochemistry of the hydration supports the assumption that the metal-coordinated carbon atom in $Fe{=}CH_2$ is nucleophilic (Schrock-like). The mechanism of the process is open to speculation. One possible mechanism would involve activation of the water via the coordinatively unsaturated iron followed by carbene insertion into the Fe–H bond.

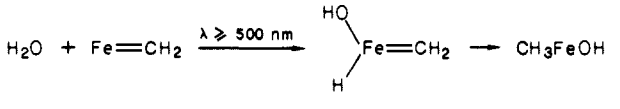

Curiously, N_2FeCH_2 was found to be less reactive toward water than $FeCH_2$, as indicated by the small change in intensity of N_2FeCH_2 bands.

The water reaction with $FeCH_2$ also provides an easy way to make various isotopically labeled CH_3FeOH species. The observed frequencies of CH_3FeOH, CH_2DFeOD, and CD_3FeOD in argon

(12) Park, M.; Hauge, R. H.; Kafafi, Z. H.; Margrave, J. L. *Chem. Commun.* **1985**, 1570.

Table VII. Measured Infrared Frequencies (cm^{-1}) of CH_3FeOH, CH_2DFeOD, and CD_3FeOD in Solid Argon

vibrational mode	CH_3FeOH	CH_2DFeOD	CD_3FeOD
O–H, O–D stretch	3744.8	2759.4	2759.5
	3744.8[a]		2759.6
Fe–O stretch	687.3	671.8	668.0
	687.5[a]		667.3

[a] Measured values from the reaction of iron atoms and methanol in solid argon.[12]

Table VIII. Measured Infrared Frequencies (cm^{-1}) of $(N_2)_xFeCH_2$, $(N_2)_xFe^{13}CH_2$, $(N_2)_xFeCHD$, and $(N_2)_xFeCD_2$ in Solid Nitrogen

vibrational mode	$(N_2)_x$-$FeCH_2$	$(N_2)_x$-$Fe^{13}CH_2$	$(N_2)_x$-FeCHD	$(N_2)_x$-$FeCD_2$
CH_2, CD_2 s stretch CD stretch of CHD	2882.1	2876.3		
CH_2, CD_2, CHD bend	1319.3	1311.0	1177.6	1002.8
Fe=C, Fe=^{13}C stretch	618.8	604.8	608.2	574.2
CH_2, CD_2 a stretch CH stretch of CHD	2941.4	2930.1	2908.6	
CH_2, CD_2, CHD wag	735.5	730.2		582.2

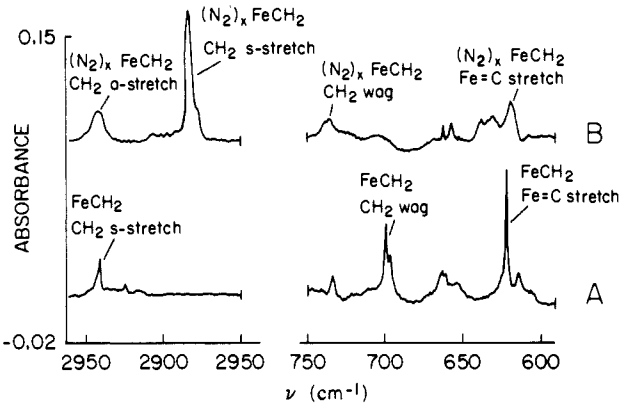

Figure 7. FTIR spectra of selected regions of (A) $FeCH_2$, N_2FeCH_2 in an argon matrix; (B) $(N_2)_xFeCH_2$ in a nitrogen matrix.

Scheme I

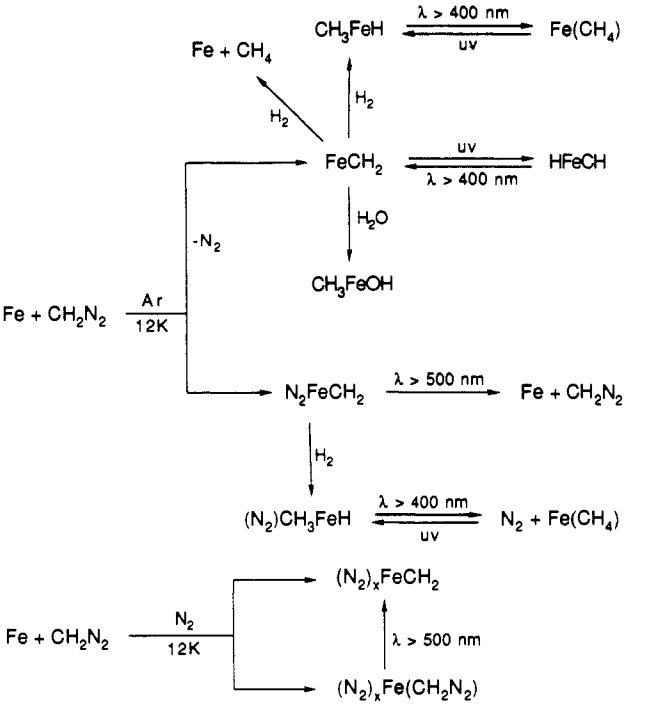

Table IX. Measured Infrared Frequencies (cm^{-1}) of Diazomethane and Iron-Diazomethane Complex in Solid Nitrogen

vibrational mode		$Fe(CH_2N_2)$	$Fe(^{13}CH_2N_2)$	$Fe(CHDN_2)$	$Fe(CD_2N_2)$
CH_2, CD_2[a]	A	427.2	419.0	390.3	337.7
CHD	B	784.4		797.3	
wag		831.4	825.0		
C=N, ^{13}C=N	A	1406.6	1397.4	1303.4	1211.6
stretch	B	1385.1	1377.2	1247.0	1050.0
CH_2, CD_2	A	3068.4	3063.6	2327.9	2236.8
s stretch	B	2900.7	2893.9		
CHD		2906.7	2899.0		
CD stretch					
CH_2, CD_2	A	3181.0	3169.2	3130.6	2407.9
a stretch	B	2966.0	2956.0	2948.0	
CHD		2972.0	2963.0		
CH stretch		2977.0	2967.0		

[a] A = CH_2N_2, B = $Fe(CH_2N_2)$.

matrices are listed in Table VII.

Finally, iron atoms react spontaneously with diazomethane in nitrogen matrices to yield a set of frequencies thought to arise from $(N_2)_xFeCH_2$ species. Although the N≡N stretching region is complicated by $Fe_2(N_2)_x$ bands, the absence of absorptions in the 1800-cm^{-1} region indicates that no "side-on" $(N_2)_xFeCH_2$ species are formed.

A selected region of the infrared spectrum of $(N_2)_xFeCH_2$ is presented in Figure 7 along with $FeCH_2$ and N_2FeCH_2 in an argon matrix. The frequencies of $(N_2)_xFeCH_2$ and the isotopically labeled species are tabulated in Table VIII.

$Fe(CH_2N_2)$ complexes, better described as $(N_2)_xFe(CH_2N_2)$, were also found in nitrogen matrices. They lead to $(N_2)_xFeCH_2$ species after $\lambda \geq 500$ nm photolysis. The absorption frequencies of these species are presented in Table IX.

The iron/diazomethane reactions in cryogenic matrices can be summarized as shown in Scheme I.

Finally, we have demonstrated that ternary reactions can be investigated readily using matrix isolation spectroscopy, suggesting that a large number of fundamental organometallic processes can be investigated using the technique.

Acknowledgment. We gratefully acknowledge The Robert A. Welch Foundation and the 3M Co. for support of this work.

Registry No. CH_3FeH, 83615-51-4; $(N_2)CH_3FeH$, 115912-13-5; $^{13}CH_3FeH$, 115912-24-8; $(N_2)^{13}CH_3FeH$, 115912-14-6; CH_2DFeD, 115912-25-9; $(N_2)CH_2DFeD$, 115912-15-7; CD_2HFeH, 115912-26-0; $(N_2)CD_2HFeH$, 115912-16-8; CD_3FeD, 115912-27-1; $(N_2)CD_3FeD$, 115912-17-9; Fe, 7439-89-6; CH_4, 74-82-8; H_2, 1333-74-0; $^{13}CH_4$, 6532-48-5; $Fe^{13}CH_2$, 115912-28-2; N_2FeCH_2, 115912-18-0; $FeCH_2$, 95250-85-4; D_2, 7782-39-0; $FeCD_2$, 115912-29-3; N_2FeCD_2, 115941-34-9; CH_3FeOH, 115912-30-6; CH_2DFeOD, 115912-31-7; CD_3FeOD, 115912-32-8; $N_2Fe^{13}CH_2$, 115912-19-1; N_2FeCHD, 115912-20-4; FeCHD, 115941-35-0; CH_2N_2, 334-88-3; HFeCH, 115912-21-5; $HFe^{13}CH$, 115912-22-6; DFeCD, 115912-23-7.

Association of Dimethyl Sulfide Radical Cation with Dimethyl Sulfide. Strength of a Two-Center Three-Electron Bond

A. J. Illies,* P. Livant, and M. L. McKee

Contribution from the Department of Chemistry, Auburn University, Auburn, Alabama 36849-5312. *Received March 31, 1988*

Abstract: A mass spectrometer designed to study gas-phase ion–molecule association equilibria was used to measure $\Delta G°$ for the reaction of $(CH_3)_2S$ (**1**) with $(CH_3)_2S^+$ (**2**) to give $[(CH_3)_2S{-}S(CH_3)_2]^+$ (**3**). The sulfur–sulfur bond in **3** is an example of a two-center three-electron (2c 3e) bond. From the measured $\Delta G°$ of −13.4 kcal/mol at 252 °C a bond strength ($\Delta H°$) of −23.9 to −26.5 kcal/mol was estimated, assuming a $\Delta S°$ of −20 to −25 cal/mol·K. In addition, a study of other ion–molecule reactions occurring in the **1** + **2** system was performed. Ab initio calculations were performed on **1**–**3** at the [PMP2/6-31G*]//3-21G(*) level, on SF_2, SF_2^+, and $[F_2S{-}SF_2]^+$ at the [PMP2/6-31G*]//3-21G(*) level, and on H_2S, H_2S^+, and $[H_2S{-}SH_2]^+$ at the PMP4SDTQ/6-31G*//3-21G(*) + zero-point correction level. The latter calculation gave $\Delta H° = -26.2$ kcal/mol for $H_2S + H_2S^+ \rightarrow [H_2S{-}SH_2]^+$. A $\Delta H°$ of −27.4 kcal/mol for **1** + **2** → **3** was calculated. This value of $\Delta H°$ was modified by including corrections taken from the higher level $H_2S + H_2S^+$ calculation to give $\Delta H° = -25.5$ kcal/mol, which agrees with the values derived from the experiment. In the $SF_2 + SF_2^+ \rightarrow [F_2S{-}SF_2]^+$ system a $\Delta H°$ of −12.2 kcal/mol was calculated.

Two-center three-electron (2c 3e) bonds have been the subject of considerable recent experimental and theoretical interest, especially 2c 3e sulfur–sulfur bonds.[1] Clark[2] has very recently published a theoretical description of odd-electron σ bonds and provided an extensive survey of the literature, which will not be repeated here. The focus in the present paper is on 2c 3e sulfur–sulfur bonding, exclusively. The 2c 3e sulfur–sulfur bond that would appear to be "simplest" is that produced by bonding of H_2S to the H_2S radical cation. However, the possibility (see below) that the $[H_2S{-}{-}SH_2]^+$ "dimer" may be bound by a proton (viz. $[H{-}S{-}H{-}{-}SH_2]^+$) instead of by a S–S 3e bond makes it desirable to study an example free of such complications. The simplest example is shown in eq 1, the reaction of dimethyl sulfide radical cation (**2**) with dimethyl sulfide (**1**).

$$\underset{\mathbf{1}}{(CH_3)_2S} + \underset{\mathbf{2}}{(CH_3)_2S^+} \rightleftarrows \underset{\mathbf{3}}{[(CH_3)_2S{-}{-}S(CH_3)_2]^+} \quad (1)$$

Reaction 1 is a prototype for the formation of the dimeric radical cations observed by ESR for a variety of sulfides, **4**,[3] and

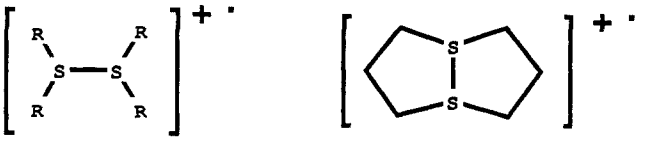

4 **5**

(1) (a) Asmus, K.-D. *Acc. Chem. Res.* **1979**, *12*, 436. (b) Glass, R. S.; Hojjatie, M.; Petsom, A.; Wilson, G. S.; Göbl, M.; Mahling, S.; Asmus, K.-D. *Phosphorus Sulfur* **1985**, *23*, 143–168. (c) For a recent paper with many leading references, see: Drewello, T.; Lebrilla, C. B.; Schwarz, H.; deKoning, L. J.; Fokkens, R. H.; Nibbering, N. M. M.; Anklam, E.; Asmus, K.-D. *J. Chem. Soc., Chem. Commun.* **1987**, 1381–1383.

(2) Clark, T. *J. Am. Chem. Soc.* **1988**, *110*, 1672–1678.

0002-7863/88/1510-7980$01.50/0